


Evidence of Quadrupole and Octupole Deformations in $^{96}\text{Zr} + ^{96}\text{Zr}$ and $^{96}\text{Ru} + ^{96}\text{Ru}$ Collisions at Ultrarelativistic Energies

Chunjian Zhang¹ and Jiangyong Jia^{1,2,*}

¹*Department of Chemistry, Stony Brook University, Stony Brook, New York 11794, USA*

²*Physics Department, Brookhaven National Laboratory, Upton, New York 11976, USA*

 (Received 30 September 2021; accepted 9 December 2021; published 11 January 2022)

In the hydrodynamic model description of heavy-ion collisions, the elliptic flow v_2 and triangular flow v_3 are sensitive to the quadrupole deformation β_2 and octupole deformation β_3 of the colliding nuclei. The relations between v_n and β_n have recently been clarified and were found to follow a simple parametric form. The STAR Collaboration has just published precision v_n data from isobaric $^{96}\text{Ru} + ^{96}\text{Ru}$ and $^{96}\text{Zr} + ^{96}\text{Zr}$ collisions, where they observe large differences in central collisions $v_{2,\text{Ru}} > v_{2,\text{Zr}}$ and $v_{3,\text{Ru}} < v_{3,\text{Zr}}$. Using a transport model simulation, we show that these orderings are a natural consequence of $\beta_{2,\text{Ru}} \gg \beta_{2,\text{Zr}}$ and $\beta_{3,\text{Ru}} \ll \beta_{3,\text{Zr}}$. We reproduce the centrality dependence of the v_2 ratio qualitatively and v_3 ratio quantitatively and extract values of β_2 and β_3 that are consistent with those measured at low-energy nuclear structure experiments. STAR data provide the first direct evidence of strong octupole correlations in the ground state of ^{96}Zr in heavy-ion collisions. Our analysis demonstrates that flow measurements in high-energy, heavy-ion collisions, especially using isobaric systems, are a new precision tool to study nuclear structure physics.

DOI: 10.1103/PhysRevLett.128.022301

Most atomic nuclei present intrinsic deformed shapes, characterized notably by quadrupole, octupole, and hexadecapole components [1,2]. Experimental evidences for nuclear deformation are primarily extracted from spectroscopic measurements and models of reduced transition probability between low-lying rotational states, which involves nuclear experiments with energy per nucleon less than a few tens of MeVs. Recently, the prospects of probing the nuclear deformation at much higher beam energy, energy per nucleon exceeding hundreds of GeVs, by taking advantage of the responses of hydrodynamic collective flow of the final state particles to the shape and sizes of the initial state, have been discussed [3–13], and several experimental evidences have been observed [14–18].

Nuclear deformation is often described by a nucleon density in a deformed Woods-Saxon form,

$$\rho(r, \theta, \phi) = \frac{\rho_0}{1 + e^{[r-R(\theta, \phi)]/a}},$$

$$R(\theta, \phi) = R_0(1 + \beta_2 Y_2^0 + \beta_3 Y_3^0 + \beta_4 Y_4^0), \quad (1)$$

where the nuclear surface $R(\theta, \phi)$ includes only the most relevant axial symmetric quadrupole, octupole, and hexadecapole deformations [19].

It is straightforward to see why dynamics of heavy-ion collisions is sensitive to nuclear deformation. These high-energy collisions deposit a large amount of energy in the overlap region, forming a hot and dense quark-gluon plasma (QGP) [20], whose initial shape in the

transverse plane is sensitive to the nuclear deformation. This initial shape is characterized via eccentricities $\varepsilon_n = |\int r^n e^{in\phi} e(r, \phi) r dr d\phi| / \int r^n e(r, \phi) r dr d\phi$, estimated from the energy density $e(r, \phi)$ in the overlap. Driven by the pressure gradient forces and subsequent hydrodynamic collective expansion, the initial ε_n are transferred into azimuthal anisotropy of final state hadrons [21], dominated by an elliptic and a triangular modulation of particle distribution, $dN/d\phi \propto 1 + 2v_2 \cos 2(\phi - \Psi_2) + 2v_3 \cos 3(\phi - \Psi_3)$. The v_n coefficients reflect hydrodynamic response of the QGP to ε_n and follow an approximate linear relation $v_n = k_n \varepsilon_n$ for events in fixed centrality [22,23]. In collisions of spherical nuclei, ε_2 mainly reflects the elliptic shape of the overlap controlled by the impact parameter, while nonzero ε_3 arises from random fluctuations of nucleons. The presence of nonzero β_n enhances ε_n and, consequently, the values of v_n , which on general ground follow a simple quadratic form [24] for $n = 2$ and 3,

$$\varepsilon_n^2 = a'_n + \sum_{m,k=2}^4 b'_{n;mk} \beta_m \beta_k,$$

$$v_n^2 = a_n + \sum_{m,k=2}^4 b_{n;mk} \beta_m \beta_k, \quad (2)$$

where ε_n^2 and v_n^2 are mean-square values calculated for events in a narrow centrality. The a'_n and a_n are values for collisions of spherical nuclei, which are strong functions of

system size and centrality. In contrast, the coefficients b' and b are expected to be nearly independent of system size [12,24]. This is because deformations change the distribution of nucleons in the entire nucleus; the coefficients in a given centrality depend mainly on the alignment of two nuclei and centrality, not the system size.

All the b' and b terms are not equally important. In fact, in the ultracentral collisions (UCCs), model studies show that only one deformation term is important [12],

$$\varepsilon_n^2 = a'_n + b'_n \beta_n^2, \quad v_n^2 = a_n + b_n \beta_n^2. \quad (3)$$

These simple relations provide a powerful data-driven method to constrain the β_2 and β_3 by comparing collisions of two species with similar sizes; see Refs. [10–12] for details. The most straightforward scenario is to consider collisions of two isobaric systems $X + X$ and $Y + Y$ with the same mass number, therefore having the same coefficients in Eq. (3). In this case, these ratios have a particularly simple expression,

$$\begin{aligned} \frac{\varepsilon_{n,Y}^2}{\varepsilon_{n,X}^2} &= 1 + \frac{b'_n}{a'_n} (\beta_{n,Y}^2 - \beta_{n,X}^2) / \left(1 + \frac{b'_n}{a'_n} \beta_{n,X}^2 \right) \\ &\approx 1 + \frac{b'_n}{a'_n} (\beta_{n,Y}^2 - \beta_{n,X}^2), \end{aligned} \quad (4)$$

$$\begin{aligned} \frac{v_{n,Y}^2}{v_{n,X}^2} &= 1 + \frac{b_n}{a_n} (\beta_{n,Y}^2 - \beta_{n,X}^2) / \left(1 + \frac{b_n}{a_n} \beta_{n,X}^2 \right) \\ &\approx 1 + \frac{b_n}{a_n} (\beta_{n,Y}^2 - \beta_{n,X}^2). \end{aligned} \quad (5)$$

The relative ordering of v_n in the two systems is a direct reflection of the ordering of their β_n values [10]. Additionally, in the UCC region, the values of a'_n and a_n are the smallest and the influence of deformations is the largest.

In this Letter, we apply this idea to the recent isobar $^{96}_{40}\text{Zr} + ^{96}_{40}\text{Zr}$ and $^{96}_{44}\text{Ru} + ^{96}_{44}\text{Ru}$ collisions [25] and make predictions on ratios of v_n from the known values of β_2 and β_3 from nuclear structure measurements, as given in Table I. Assuming the same β_n for neutrons and protons and a uniform charge distribution out to the distance $R(\theta, \phi)$, the β_n values are obtained from the measured

TABLE I. Values of β_2 deduced from the $B(E2; 0_1^+ \rightarrow 2_1^+)$ [32] and β_3 deduced from three $B(E3; 0_1^+ \rightarrow 3_1^-)$ [33] transition measurements via Eq. (6). The corresponding excitation energies are also provided. In general, larger excitation energy corresponds to smaller deformability for the nucleus.

	β_2	$E_{2_1^+}$ (MeV)	β_3	$E_{3_1^-}$ (MeV)
^{96}Ru	0.154	0.83	...	3.08
^{96}Zr	0.062	1.75	0.202, 0.235, 0.27	1.90

reduced electric transition probability $B(E_n)\uparrow$ via the standard formula [26],

$$\beta_2 = \frac{4\pi}{3ZR_0^2} \sqrt{\frac{B(E2)\uparrow}{e^2}}, \quad \beta_3 = \frac{4\pi}{3ZR_0^3} \sqrt{\frac{B(E3)\uparrow}{e^2}}, \quad (6)$$

with $R_0 = 1.2A^{1/3}$ fm. We note that the number of neutrons in ^{96}Zr nucleus is equal to one of the so-called ‘‘octupole magic’’ numbers 56 [27]. Low-energy experiments indeed show that ^{96}Zr has a very large octupole collectivity corresponding to a large β_3 value, but a small β_2 value [28–30]. On the other hand, the ^{96}Ru nucleus has larger β_2 , but shows no evidence of significant β_3 . The latter is expected from the very large excitation energy for its 3_1^- state. In this analysis, we assume $\beta_{3,\text{Ru}} = 0$. Note that the predictions from nuclear structure models [31] have large discrepancies from these data; therefore, they are not used in this Letter.

To understand the hydrodynamic response to nuclear deformations and make predictions, we employ a multi-phase transport (AMPT) model [34] as a proxy for hydrodynamics. This model is successful in describing collective flow data in small and large collision systems at RHIC and LHC [35–38] and has been used to study the β_n dependence of v_n [10,11]. We use AMPT model v2.26t5 in string-melting mode at $\sqrt{s_{\text{NN}}} = 200$ GeV and a partonic cross section of 3.0 mb [36,37], which gives a reasonable description of Au + Au and U + U v_2 data at RHIC [39,40]. We simulate generic isobar $^{96}\text{X} + ^{96}\text{X}$ collisions with $R_0 = 5.09$ and $a = 0.52$ fm. We performed a scan on β_2 : $\beta_2 = 0, 0.05, 0.1, 0.15, 0.2$ and $\beta_3 = 0$, as well as a scan on β_3 : $\beta_3 = 0, 0.05, 0.1, 0.15, 0.2$ and $\beta_2 = 0.06$. The ε_n are calculated from participating nucleons and v_n are calculated using two-particle correlation method with hadrons in $0.2 < p_T < 2$ GeV and $|\eta| < 2$ [41].

The left panels of Fig. 1 show ratios of $\varepsilon_n(\beta_2, \beta_3)$ for given values of β_2 or β_3 to that for spherical nuclei. There are four different types of ratios considered: $\varepsilon_3(\beta_2, 0)/\varepsilon_2(0, 0)$, $\varepsilon_3(0, \beta_3)/\varepsilon_3(0, 0)$, $\varepsilon_2(0, \beta_3)/\varepsilon_2(0, 0)$, and $\varepsilon_3(\beta_2, 0)/\varepsilon_3(0, 0)$; i.e., we not only consider how the ε_n are affected by β_n but also the cross-correlation between ε_2 and β_3 or between ε_3 and β_2 . Our study shows that the ε_n in the Glauber model takes the following simplified version of Eq. (2) [12]:

$$\varepsilon_2^2 = a'_2 + b'_2 \beta_2^2 + b'_{2,3} \beta_3^2, \quad \varepsilon_3^2 = a'_3 + b'_3 \beta_3^2. \quad (7)$$

The ε_2 is strongly influenced by β_3 in the noncentral collisions, reaching a maximum at $N_{\text{part}} \sim 146$ corresponding to about 8% centrality. The right panels of Fig. 1 show ratios of v_n^2 with the same layout, which we found can be well parametrized by

$$v_2^2 = a_2 + b_2\beta_2^2 + b_{2,3}\beta_3^2, \quad v_3^2 = a_3 + b_3\beta_3^2. \quad (8)$$

It is clear from Fig. 1 that the ratio of v_n in all cases is smaller than the ratio of ε_n for the same β_n . This observation implies that the hydrodynamic response for b' parameters are smaller than those for the a' , i.e., $b_n/b'_n < a_n/a'_n$ and $b_{2,3}/b'_{2,3} < a_2/a'_2$. In other words, the contributions of v_n from nuclear deformation are more damped by hydrodynamic evolution than that from the eccentricity of the spherical nuclei. One possible explanation is that the

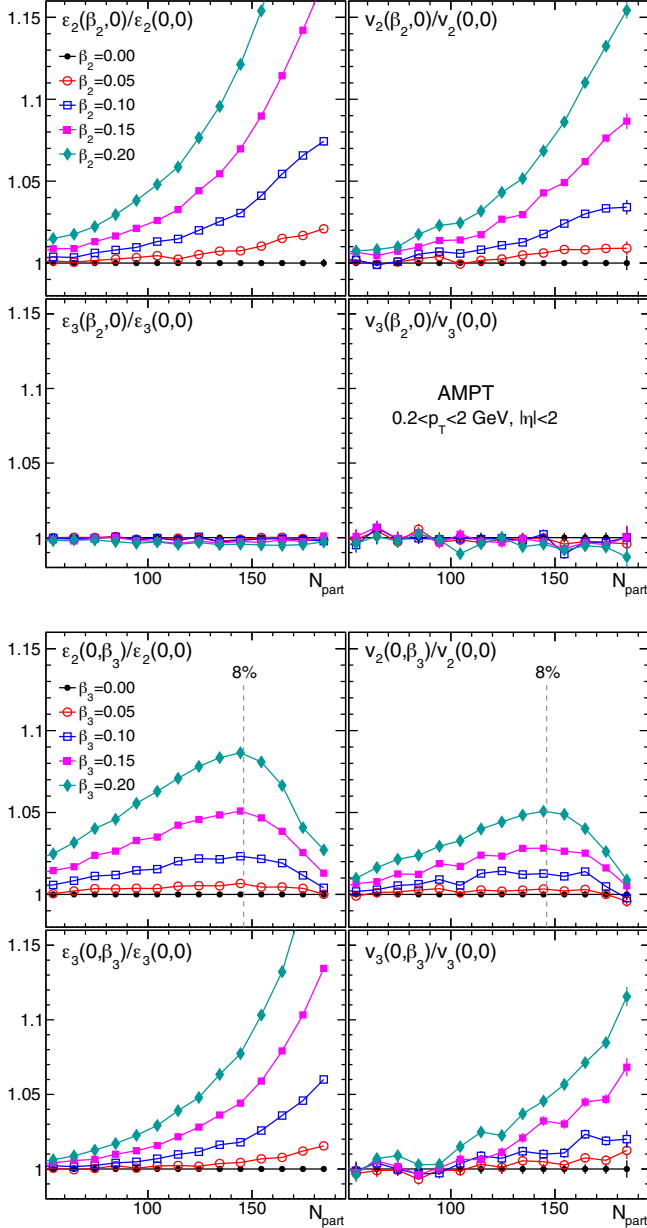


FIG. 1. The N_{part} dependence of ratios of ε_n (left) or v_n (right) relative to undeformed case with for $n = 2, 3$ in generic ${}^{96}\text{X} + {}^{96}\text{X}$ collisions with different β_2 (top) and β_3 (bottom) values. The v_n are calculated in the AMPT models with hadrons in $|\eta| < 2$ and $0.2 < p_T < 2$ GeV.

nuclear deformation increases ε_n by adding more nucleons toward the edge of the overlap, leading to a weaker hydrodynamic response and less efficient conversion of ε_n to v_n .

With Eq. (7) in hand and using the values of β_n from Table I, we are ready to predict the v_n ratios between Ru + Ru and Zr + Zr collisions. Safely assuming $\beta_{3,\text{Ru}} = 0$, these ratios are expected to scale like

$$\frac{v_{2,\text{Ru}}^2}{v_{2,\text{Zr}}^2} \approx 1 + \frac{b_2}{a_2} (\beta_{2,\text{Ru}}^2 - \beta_{2,\text{Zr}}^2) - \frac{b_{2,3}}{a_2} \beta_{3,\text{Zr}}^2, \quad (9)$$

$$\frac{v_{3,\text{Ru}}^2}{v_{3,\text{Zr}}^2} \approx 1 - \frac{b_3}{a_3} \beta_{3,\text{Zr}}^2. \quad (10)$$

The coefficients b_n/a_n and $b_{2,3}/a_2$ can be calculated from Fig. 1 as a function of N_{part} , which can then be used to predict $v_{n,\text{Ru}}/v_{n,\text{Zr}}$. Alternatively, $v_{n,\text{Ru}}/v_{n,\text{Zr}}$ can be obtained directly according to the β_n values in Table I,

$$\begin{aligned} \frac{v_{n,\text{Ru}}}{v_{n,\text{Zr}}} &\approx \frac{v_n(\beta_{2,\text{Ru}}, 0)}{v_n(\beta_{2,\text{Zr}}, 0)} \times \frac{v_n(0, \beta_{3,\text{Ru}})}{v_n(0, \beta_{3,\text{Zr}})} \\ &= \frac{v_n(0.154, 0)}{v_n(0.062, 0)} \times \frac{v_n(0, 0)}{v_n(0, 0.2)}. \end{aligned}$$

Since $\beta_{2,\text{Ru}} \gg \beta_{2,\text{Zr}}$ and the value of $\beta_{3,\text{Zr}}$ is large, the ratio $v_{2,\text{Ru}}/v_{2,\text{Zr}}$ is expected to contain a positive contribution from β_2 and a negative contribution from β_3 . This is clearly demonstrated in the top panel of Fig. 2. The $\beta_{3,\text{Zr}}$ has a small impact in the 0%–1% centrality, but significantly reduces the v_2 ratio over the 1%–40% centrality range, with the maximum reduction at around $N_{\text{part}} \sim 146$ or 8% centrality. The influence of $\beta_{3,\text{Zr}}$ also forces a much sharper decrease of the v_2 ratio in the centrality range of 0%–5% and leads to a nonmonotonic centrality dependence. On the other hand, the predicted $v_{3,\text{Ru}}/v_{3,\text{Zr}}$ ratios in the bottom panel of Fig. 2 are independent of the β_2 of the two systems. This interesting interplay between β_2 and β_3 and the resulting features in the v_n ratio in the isobar collisions are salient and robust predictions that can be verified experimentally.

The STAR Collaboration has just released the $v_{n,\text{Ru}}/v_{n,\text{Zr}}$ data in several coarse centrality bins [25]; they are contrasted with our predictions in Fig. 2. The v_2 ratio data show nonmonotonic centrality dependence similar in shape to our prediction, which include effects of both β_2 and β_3 , and such nonmonotonicity was not predicted in previous studies that did not include the influence of β_3 [42,43]. However, our prediction is systematically lower than the STAR data by up to 2% in the midcentral and peripheral region. This residual difference could be due to the large neutron skin effect in ${}^{96}\text{Zr}$ [43], which was found to enhance $\varepsilon_{2,\text{Ru}}/\varepsilon_{2,\text{Zr}}$ with a shape and magnitude similar to this difference. Remarkably, our prediction of v_3 ratio agrees nearly perfectly with the STAR data over the entire

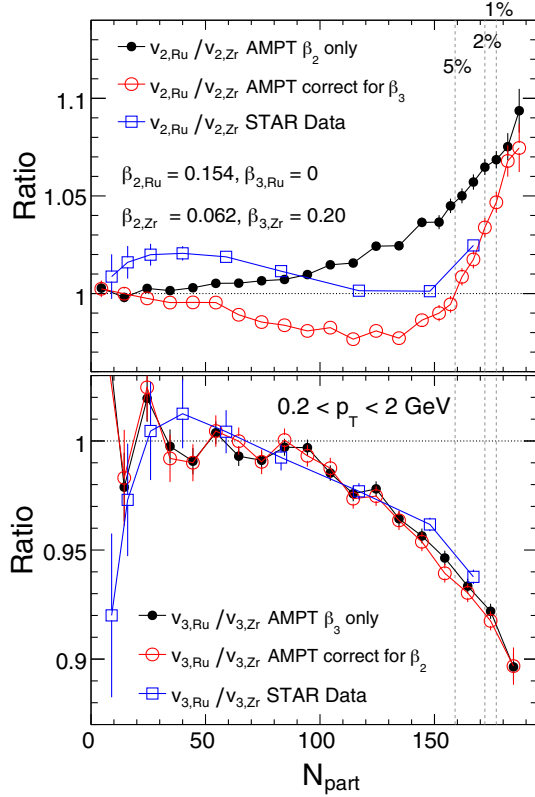


FIG. 2. Predicted ratios of v_2 (top) and v_3 (bottom) between Ru + Ru and Zr + Zr collisions from the AMPT model based on the β_2 and β_3 values for Ru and Zr from Table I. They are compared with the STAR data from Ref. [25].

centricity range when $\beta_{3,Zr} = 0.2$ is used. This also raises a question whether the large β_3 value constrained by the isobar collisions could imply a large static octupole deformation in the ground state of ^{96}Zr , as implemented in our AMPT model simulation.

Next, we make predictions in the 0%–1% most central collisions, where the influence of nuclear deformation is strongest, the contribution from β_3 to v_2 is small, and v_n ratios are expected to be described precisely by Eq. (5) with b_n/a_n as the only free parameters. The STAR data are not yet available in this region. Figure 3 shows the predicted ratios $v_{2,Ru}^2/v_{2,Zr}^2$ and $v_{3,Ru}^2/v_{3,Zr}^2$ as a function of $\beta_{2,Ru}^2$ and $\beta_{3,Zr}^2$, respectively. The predictions follow strictly a linear dependence on β_n^2 . Assuming the $\beta_{2,Ru} = 0.154$ and $\beta_{2,Zr} = 0.062$ from Table I, we predict a $v_{2,Ru}^2/v_{2,Zr}^2 \approx 1.16$, corresponding to $v_{2,Ru}/v_{2,Zr} \approx 1.08$. On the other hand, the three octupole deformation values from nuclear structure measurements, $\beta_{3,Zr} = 0.202, 0.235, 0.27$, would predict $v_{3,Zr}^2/v_{3,Ru}^2 = 1.24, 1.33, 1.44$ as indicated by the solid arrows in Fig. 3, or equivalently, $v_{3,Ru}/v_{3,Zr} = 0.90, 0.87, 0.83$. The latter two cases, $\beta_{3,Zr} = 0.235$ and 0.27 , are clearly ruled out by the data-theory comparison of the v_3 ratio in the bottom panel of Fig. 2. These two $\beta_{3,Zr}$ values would also lead to further reduction of the $v_{2,Ru}/v_{2,Zr}$ ratio

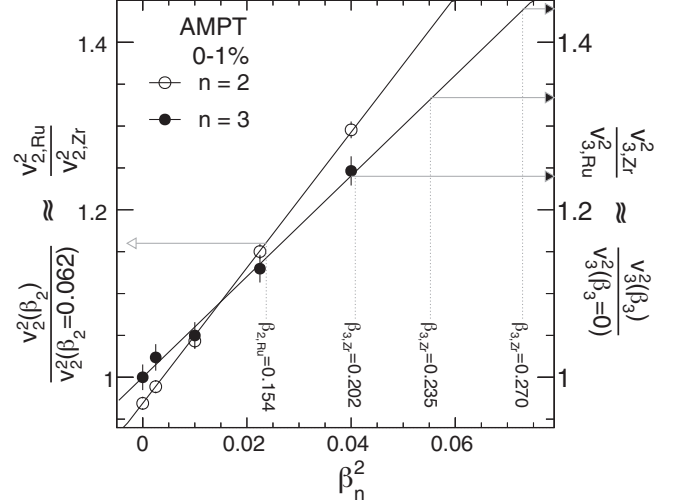


FIG. 3. Predicted ratio of $v_{2,Ru}^2/v_{2,Zr}^2$ as a function of $\beta_{2,Ru}^2$ assuming $\beta_{2,Zr} = 0.062$ (open symbols), and ratio of $v_{3,Zr}^2/v_{3,Ru}^2$ as a function of $\beta_{3,Zr}^2$ assuming $\beta_{3,Ru} = 0$ (filled symbols) from the AMPT model for the 0%–1% centrality. The arrows indicate the corresponding ratios for $\beta_{2,Ru} = 0.154$ (left pointing) and $\beta_{3,Zr} = 0.202, 0.235, \text{ and } 0.27$ from Table I (right pointing).

(indicated by the open circles) in the top panel of Fig. 2. This additional reduction amounts to $0.235^2/0.2^2 - 1 = 38\%$ or $0.27^2/0.2^2 - 1 = 82\%$ of the difference between the two AMPT predictions, which will make both the shape and the magnitude of the $v_{2,Ru}/v_{2,Zr}$ incompatible with the experimental data, even after including the predicted neutron skin effects [43]. Therefore, for the first time, the isobar collisions show clear potential for providing new constraints on nuclear deformation parameters that can complement those from nuclear structure spectroscopy in testing state-of-the-art nuclear structure models. In order to pin down the interplay between β_2 and β_3 more quantitatively, however, STAR measurement [25] should be extended to finer centrality bins, especially in the 0%–5% range where the v_n ratios are still changing very rapidly.

Some work is required in order to accomplish a precise determination of nuclear deformations using heavy-ion collisions. First, and most importantly, we need to understand the connection of the β_n given by nuclear structure method (6) and β_n in heavy-ion collisions via Eq. (1). The former measures the charge distribution at the timescale of 10^{-21} s, while the heavy-ion collisions care only about the mass distribution at a much shorter time of 10^{-24} s, which is also strongly Lorentz contracted, unlike in the low-energy experiments. For example, changing the R_0 value alone in Eq. (6) would directly change the value of extracted β_n , but changing the R_0 in Eq. (1) has little impact on the hydrodynamic response to β_n . From the modeling side of the heavy-ion collisions, we need to pin down the hydrodynamic response of v_n to the deformation contribution to the eccentricity, which is clearly different from the hydrodynamic response of v_n to the baseline

eccentricity for spherical nuclei (see Fig. 1). Further hydrodynamic model studies are required to quantify the systematic uncertainties, in particular, the ratio a_n/b_n . Nevertheless, the STAR results and our study demonstrate that heavy-ion collisions can serve as a new tool for imaging the shape of the atomic nuclei and possibly other features of their nuclear structure. This provides good arguments for an extended system scan of different isobaric systems for precision measurement of interesting nuclear structure effects and complements the low-energy methods [11,12].

In summary, recent STAR measurement of v_2 and v_3 show significant differences between $^{96}\text{Zr} + ^{96}\text{Zr}$ and $^{96}\text{Ru} + ^{96}\text{Ru}$ collisions. Using a transport simulation, we show that these differences can be naturally explained from the large quadrupole deformation β_2 of ^{96}Ru and large octupole deformation β_3 of ^{96}Zr . Our calculations quantitatively describe the $v_{3,\text{Ru}}/v_{3,\text{Zr}}$ by assuming $\beta_{3,\text{Zr}} = 0.2$ from one nuclear structure measurement. However, the presence of $\beta_{3,\text{Zr}}$ was found to significantly enhance the $v_{2,\text{Zr}}$ and led to a nonmonotonic centrality dependence of $v_{2,\text{Ru}}/v_{2,\text{Zr}}$ as observed in the data. Additional physics such as neutron skin differences are also required to quantitatively describe the v_2 ratio. Our analysis demonstrates that isobaric heavy-ion collisions can be used as a precision tool to image the shape and radial structures of the nuclei. We hope this can be done in the existing high-energy collider facilities in the near future.

We thank Yu Hu for providing the STAR data. We thank Giuliano Giacalone for valuable suggestions. We acknowledge Somadutta Bhatta for helpful discussions. This work is supported by DOE Award No. DEFG0287ER40331.

*Corresponding author.

jiangyong.jia@stonybrook.edu

- [1] K. Heyde and J.L. Wood, Shape coexistence in atomic nuclei, *Rev. Mod. Phys.* **83**, 1467 (2011).
- [2] K. Heyde and J.L. Wood, Nuclear shapes: From earliest ideas to multiple shape coexisting structures, *Phys. Scr.* **91**, 083008 (2016).
- [3] U. W. Heinz and A. Kuhlman, Anisotropic Flow and Jet Quenching in Ultrarelativistic U + U Collisions, *Phys. Rev. Lett.* **94**, 132301 (2005).
- [4] P. Filip, R. Lednicky, H. Masui, and N. Xu, Initial eccentricity in deformed $^{197}\text{Au} + ^{197}\text{Au}$ and $^{238}\text{U} + ^{238}\text{U}$ collisions at $\sqrt{s_{\text{NN}}} = 200$ GeV at the BNL relativistic heavy ion collider, *Phys. Rev. C* **80**, 054903 (2009).
- [5] Q. Y. Shou, Y. G. Ma, P. Sorensen, A. H. Tang, F. Videbæk, and H. Wang, Parameterization of deformed nuclei for Glauber modeling in relativistic heavy ion collisions, *Phys. Lett. B* **749**, 215 (2015).
- [6] A. Goldschmidt, Z. Qiu, C. Shen, and U. Heinz, Collision geometry and flow in uranium + uranium collisions, *Phys. Rev. C* **92**, 044903 (2015).
- [7] G. Giacalone, J. Noronha-Hostler, M. Luzum, and J.-Y. Ollitrault, Hydrodynamic predictions for 5.44 TeV Xe + Xe collisions, *Phys. Rev. C* **97**, 034904 (2018).
- [8] G. Giacalone, Elliptic flow fluctuations in central collisions of spherical and deformed nuclei, *Phys. Rev. C* **99**, 024910 (2019).
- [9] G. Giacalone, J. Jia, and V. Somà, Accessing the shape of atomic nuclei with relativistic collisions of isobars, *Phys. Rev. C* **104**, L041903 (2021).
- [10] G. Giacalone, J. Jia, and C. Zhang, The Impact of Nuclear Deformation on Relativistic Heavy-Ion Collisions: Assessing Consistency in Nuclear Physics across Energy Scales, *Phys. Rev. Lett.* **127**, 242301 (2021).
- [11] J. Jia, S. Huang, and C. Zhang, Probing nuclear quadrupole deformation from correlation of elliptic flow and transverse momentum in heavy ion collisions, [arXiv:2105.05713](https://arxiv.org/abs/2105.05713) [Phys. Rev. C (to be published)].
- [12] J. Jia, Shape of atomic nuclei in heavy ion collisions, [arXiv:2106.08768](https://arxiv.org/abs/2106.08768) [Phys. Rev. C (to be published)].
- [13] B. Bally, M. Bender, G. Giacalone, and V. Somà, Evidence of the triaxial structure of ^{129}Xe at the Large Hadron Collider, [arXiv:2108.09578](https://arxiv.org/abs/2108.09578).
- [14] L. Adamczyk *et al.* (STAR Collaboration), Azimuthal Anisotropy in U + U and Au + Au Collisions at RHIC, *Phys. Rev. Lett.* **115**, 222301 (2015).
- [15] S. Acharya *et al.* (ALICE Collaboration), Anisotropic flow in Xe-Xe collisions at $\sqrt{s_{\text{NN}}} = 5.44$ TeV, *Phys. Lett. B* **784**, 82 (2018).
- [16] A. M. Sirunyan *et al.* (CMS Collaboration), Charged-particle angular correlations in XeXe collisions at $\sqrt{s_{\text{NN}}} = 5.44$ TeV, *Phys. Rev. C* **100**, 044902 (2019).
- [17] G. Aad *et al.* (ATLAS Collaboration), Measurement of the azimuthal anisotropy of charged-particle production in Xe + Xe collisions at $\sqrt{s_{\text{NN}}} = 5.44$ TeV with the ATLAS detector, *Phys. Rev. C* **101**, 024906 (2020).
- [18] J. Jia, Nuclear deformation effects via Au + Au and U + U collisions from STAR, *Contribution to the VI International Conference on the Initial Stages of High-Energy Nuclear Collisions, January 2021*, <https://indico.cern.ch/event/854124/contributions/4135480/>.
- [19] Including other internal shape degrees of freedom, such as triaxiality, does not affect the two-particle observables e_n^2 and v_n^2 [12].
- [20] W. Busza, K. Rajagopal, and W. van der Schee, Heavy ion collisions: The big picture, and the big questions, *Annu. Rev. Nucl. Part. Sci.* **68**, 339 (2018).
- [21] U. W. Heinz, Towards the little bang standard model, *J. Phys. Conf. Ser.* **455**, 012044 (2013).
- [22] H. Niemi, K. J. Eskola, and R. Paatelainen, Event-by-event fluctuations in a perturbative QCD + saturation + hydrodynamics model: Determining QCD matter shear viscosity in ultrarelativistic heavy-ion collisions, *Phys. Rev. C* **93**, 024907 (2016).
- [23] B. Schenke, C. Shen, and D. Teaney, Transverse momentum fluctuations and their correlation with elliptic flow in nuclear collision, *Phys. Rev. C* **102**, 034905 (2020).
- [24] J. Jia, Probing triaxial deformation of atomic nuclei in high-energy heavy ion collisions, [arXiv:2109.00604](https://arxiv.org/abs/2109.00604).
- [25] M. Abdallah *et al.* (STAR Collaboration), Search for the chiral magnetic effect with isobar collisions at

- $\sqrt{s_{NN}} = 200$ GeV by the STAR Collaboration at the BNL Relativistic Heavy Ion Collider, *Phys. Rev. C* **105**, 014901 (2021).
- [26] *Nuclear Structure II*, edited by A. Bohr and B. R. Mottelson (World Scientific, Singapore, 1998), p. 348.
- [27] P. A. Butler and W. Nazarewicz, Intrinsic reflection asymmetry in atomic nuclei, *Rev. Mod. Phys.* **68**, 349 (1996).
- [28] M. M. Stautberg, R. R. Johnson, J. J. Kraushaar, and B. W. Ridley, The $96\text{ Zr}(p, p')$ and $96\text{ Zr}(p, d)$ reaction at 19.4 MeV, *Nucl. Phys.* **A104**, 67 (1967).
- [29] H. Mach, S. Cwiok, W. Nazarewicz, B. Fogelberg, M. Moszynski, J. Winger, and R. L. Gill, Strong octupole and dipole collectivity in Zr-96: Indication for octupole instability in the $A = 100$ mass region, *Phys. Rev. C* **42**, R811 (1990).
- [30] D. Hofer *et al.*, Direct and multiple excitations in 96 Zr from inelastic-scattering experiments, *Nucl. Phys.* **A551**, 173 (1993).
- [31] P. Möller, A. J. Sierk, T. Ichikawa, and H. Sagawa, Nuclear ground-state masses and deformations: FRDM(2012), *At. Data Nucl. Data Tables* **109–110**, 1 (2016).
- [32] B. Pritychenko, M. Birch, B. Singh, and M. Horoi, Tables of E2 transition probabilities from the first 2^+ states in even-even nuclei, *At. Data Nucl. Data Tables* **107**, 1 (2016); Erratum, *At. Data Nucl. Data Tables* **114**, 371 (2017).
- [33] T. Kibédi and R. H. Spear, reduced electric-octupole transition probabilities, $B(E3; 0_1^+ \rightarrow 3_1^-)$ an update, *At. Data Nucl. Data Tables* **80**, 35 (2002).
- [34] Z.-W. Lin, C. M. Ko, B.-A. Li, B. Zhang, and S. Pal, A Multi-phase transport model for relativistic heavy ion collisions, *Phys. Rev. C* **72**, 064901 (2005).
- [35] A. Adare *et al.* (PHENIX Collaboration), Measurements of directed, elliptic, and triangular flow in Cu + Au collisions at $\sqrt{s_{NN}} = 200$ GeV, *Phys. Rev. C* **94**, 054910 (2016).
- [36] G.-L. Ma and A. Bzdak, Long-range azimuthal correlations in proton-proton and proton-nucleus collisions from the incoherent scattering of partons, *Phys. Lett. B* **739**, 209 (2014).
- [37] A. Bzdak and G.-L. Ma, Elliptic and Triangular Flow in $p + \text{Pb}$ and Peripheral $\text{Pb} + \text{Pb}$ Collisions from Parton Scatterings, *Phys. Rev. Lett.* **113**, 252301 (2014).
- [38] M.-W. Nie, P. Huo, J. Jia, and G.-L. Ma, Multiparticle azimuthal cumulants in $p + \text{Pb}$ collisions from a multiphase transport model, *Phys. Rev. C* **98**, 034903 (2018).
- [39] J. Xu and C. M. Ko, Triangular flow in heavy ion collisions in a multiphase transport model, *Phys. Rev. C* **84**, 014903 (2011).
- [40] M. Abdallah *et al.* (STAR Collaboration), Azimuthal anisotropy measurements of strange and multistrange hadrons in $\text{U} + \text{U}$ collisions at $\sqrt{s_{NN}} = 193$ GeV at the BNL relativistic heavy ion collider, *Phys. Rev. C* **103**, 064907 (2021).
- [41] G. Aad *et al.* (ATLAS Collaboration), Measurement of the azimuthal anisotropy for charged particle production in $\sqrt{s_{NN}} = 2.76$ TeV lead-lead collisions with the ATLAS detector, *Phys. Rev. C* **86**, 014907 (2012).
- [42] W.-T. Deng, X.-G. Huang, G.-L. Ma, and G. Wang, Test the chiral magnetic effect with isobaric collisions, *Phys. Rev. C* **94**, 041901(R) (2016).
- [43] H.-j. Xu, H. Li, X. Wang, C. Shen, and F. Wang, Determine the neutron skin type by relativistic isobaric collisions, *Phys. Lett. B* **819**, 136453 (2021).